PAPER

Check for updates

Synthesis and non-isothermal crystallization kinetics of polyamide 66 copolymers containing alicyclic structures

Weijian Lu,[a] Chunhua Wang, [ID] *[a] Yong Yi,[a] Mingxi Liao,[b] Jianlin Li[a] and Wenzhi Wang*[a]

To further improve the performance of PA66 and expand its applications, a new strategy was proposed to introduce an alicyclic structure into PA66 chain by the copolymerization method. Initially, 3,3′-dimethyl-4,4′-diaminodicyclohexylmethane (MACM) was reacted with 1,6-adipic acid to form MACM6 salt, and then, it was copolymerized with PA66 salt to synthesize PA66/MACM6 copolymers with alicyclic structures. PA66/MACM6 copolymers exhibited good thermal stabilities, and the presence of alicyclic structure had no significant effect on their thermal stabilities. Notably, the crystallization temperature, crystallinity and melting point of the PA66/MACM6 copolymer decreased gradually with increasing MACM6 content, indicating that the addition of the MACM6 segment disrupted the regularity of the original PA66 chain. Moreover, as the melting point of the PA66/MACM6 copolymer was in between 223.9 °C and 254.8 °C, it could be processed in a wide temperature range to meet the requirements of different industrial applications. The non-isothermal crystallization kinetics of PA66/MACM6 copolymers were investigated using the Jeziorny and Mo methods, and the crystallization activation energy was calculated using the Kissinger method. The results indicated that the introduction of the MACM6 segment into the PA66 chain by copolymerization inhibited its crystallization and increased its crystallization activation energy, thereby reducing its crystallization rate. In addition, PA66/MACM6 copolymers exhibited improved toughness with a slight decrease in the strength. When the content of MACM6 reached 40 wt%, the elongation at break of PA66/MACM6-40 was about 760% higher than that of PA66, suggesting its high toughness.

Introduction

Polyamide 66 (PA66), one of the most important engineering plastics, has attracted extensive attention in industrial application and theoretical research owing to its excellent chemical resistance, good thermal stability, high mechanical strength, and easy processing.[1–5] As a typical semi-crystalline polymer, its crystallization behavior is primarily determined by the hydrogen bonding ability between its –NH– and –CO– groups present on adjacent molecular chains.[6] The PA66 chain contains a large number of amide groups, and thus, it has a strong hydrogen bond interaction. Moreover, the relatively regular arrangement of PA66 chains contributes to crystallization, resulting in high crystallinity and high mechanical strength. However, crystallinity is also a major factor affecting

the toughness of polyamide materials.[7–12] PA66 exhibits low toughness and brittle fracture behavior owing to its high crystallinity, which limits its application in the fields of pipe, rope, cable ties and so on. Therefore, improving the toughness of PA66 has been a focus of research in recent years.

Copolymerization method has been used in PA66 modification owing to its simplicity and high efficiency. The target PA66 copolymers with desirable properties can be synthesized by selecting suitable comonomers for molecular design. For example, Harvey *et al.* synthesized PA66/6 copolymers and found that adding PA6 segment into the PA66 backbone reduced the melting temperature, crystallization temperature and crystallinity.[13] Lin *et al.* synthesized PA66/56 copolymers *via* a one-pot polycondensation reaction of pentamethyleneammonium adipate salt and hexamethyleneammonium adipate salt in aqueous solution, which showed excellent toughness and high transparency owing to their low crystallinity and small crystal size.[14] Rwei *et al.* incorporated hexamethylenediamine and terephthalic acid into the polymerization process of PA66 to form PA66/6T copolymers. The results indicated that the formed PA66/6T copolymers were isomorphous and exhibited minor crystal difference as the addition of 6T varied from 0 to 30 mol% owing

[a] National and Local Joint Engineering Research Center of Advanced Packaging Material Research and Development Technology, School of Packaging and Materials Engineering, Hunan University of Technology, Zhuzhou 412007, Hunan, China. E-mail: wangchunhua@hut.edu.cn; wangwenzhi@hut.edu.cn

[b] School of Life Sciences and Chemistry, Hunan University of Technology, Zhuzhou 412007, China

to the similar molecular chain lengths of 66 and 6T.[15] Chen *et al.* synthesized PA66 copolymers with aromatic moieties from recycled PET waste, which exhibited excellent thermal and mechanical properties.[16] However, the modification of PA66 by introducing an alicyclic chain segment has received little attention. Recently, our research group reported the synthesis of PA66 copolymers with cyclohexyl groups using 4,4′-diaminodicyclohexylmethane (PACM), adipic acid and PA66 salt as the comonomers, wherein their films exhibited superior toughness and great optical performance.[17] It is well known that research on the crystallization kinetics of polymer materials will be helpful to improve their properties and understand their formation mechanism.[18,19] Unfortunately, there is no report on the crystallization kinetics of PA66 copolymers with alicyclic structures. In general, there are two kinds of polymer crystallization processes, namely, isothermal crystallization and non-isothermal crystallization.[20] Nevertheless, the polymer crystallization process is usually carried out under dynamic and non-isothermal conditions during practical processing, such as extrusion, injection molding, and film or fiber forming.[21–26] There is no doubt that the non-isothermal crystallization behavior of polymers has a great influence on the processing and properties of products.

In this work, 3,3′-dimethyl-4,4′-diaminodicyclohexylmethane (MACM) was selected as a large volume alicyclic diamine monomer and reacted with 1,6-adipic acid to form MACM6 salt and then copolymerized with PA66 salt to synthesize PA66/MACM6 copolymers with alicyclic structures. The structure of PA66/MACM6 copolymers was characterized by Fourier-transform infrared spectroscopy (FTIR) and proton nuclear magnetic resonance (¹H-NMR). Thermogravimetric analysis (TGA) and differential scanning calorimetry (DSC) were utilized to investigate the thermal properties of the copolymers. Based on the DSC data, the non-isothermal crystallization kinetics of the copolymers was studied using both the Jeziorny method and the Mo method, and the crystallization activation energy was calculated using the Kissinger method. The mechanical properties were researched by an electronic universal testing machine. The influence of the MACM6 segment on the thermal properties, non-isothermal crystallization behaviors, and mechanical properties of PA66/MACM6 copolymers was investigated, which could provide guidance for the development and application of subsequent products.

Materials and methods

Materials

PA66 salt (99.9%) was supplied from BASF Co., Ltd, Shanghai, China. 1,6-Adipic acid (99.8%) was purchased from Huafon Chemical Co., Ltd, Chongqing, China. 3,3′-Dimethyl-4,4′-diaminodicyclohexylmethane (MACM, 99%) was bought from Xuhua Biotechnology Co., Ltd, Shenzhen, China. Ethanol (95%) was provided by Hunan Xiangyikang Pharmaceutical Co., Ltd, Yiyang, China.

Preparation of copolymers

PA66/MACM6 copolymers can be synthesized by the salting reaction and copolymerization reaction, and their synthetic route is shown in Fig. 1. A typical procedure is described as follows. First, a certain mass of 1,6-adipic acid was added into a flask, followed by an equal mass of ethanol. After heating to 80 °C, MACM was added dropwise into the flask with stirring until the pH value of the solution reached 7.2–7.5. The solution was allowed to stand for 4 h at room temperature, and the MACM6 salt was obtained by filtration, washing and drying. Next, PA66 salt, a certain mass of MACM6 salt and distilled water, were added into an autoclave, and the solid content of the reaction system was 20 wt%. In order to remove oxygen, the reaction system was treated by vacuuming and filling with high purity N_2 three times. The reaction system was heated to 210 °C under stirring, and the pressure was kept at 1.5–2.0 MPa for 2 h. The reaction system was further heated to 270 °C, and then the exhaust valve was opened slowly to reduce the pressure to atmospheric pressure. The system was vacuumed and reacted at −0.05 MPa for 1 h. Finally, the PA66/MACM6 copolymer was
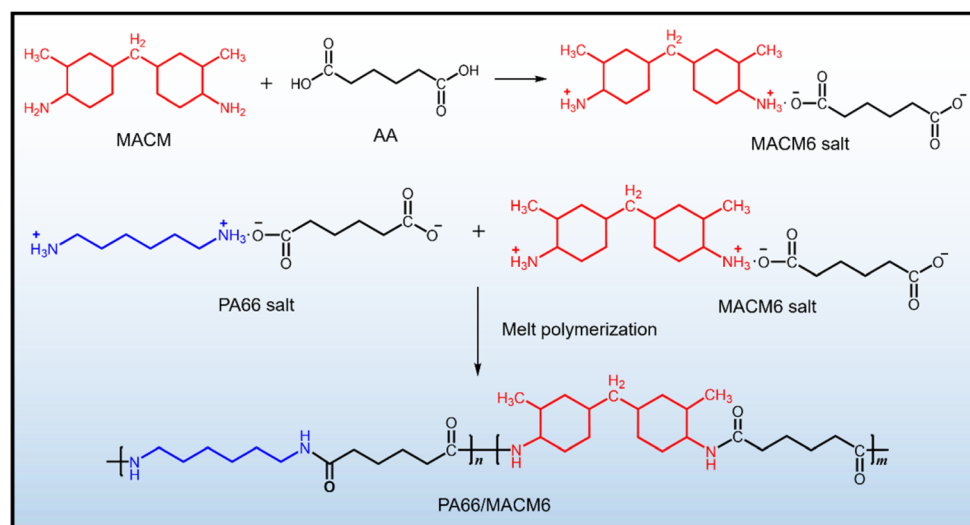

Fig. 1 Synthetic route for PA66/MACM6 copolymers.

obtained by discharging, cooling, granulating and drying. PA66/MACM6 copolymer was named as PA66/MACM6-n, where n represents the weight percentage of MACM6 salt added in the feeding salts. For comparison, pure PA66 was also synthesized by the same process.

Characterization

FTIR spectra were recorded on a Bruker Tensor 27 FTIR spectrometer (Germany) in attenuated total reflection mode from 4000 cm^{-1} to 400 cm^{-1}.

^{1}H-NMR spectra were acquired on a Bruker AVANCE III HD 600 MHz NMR spectrometer (Germany) at 25 °C using deuterated trifluoroacetic acid as a solvent.

The relative viscosity (η_r) was measured by a Ubbelohde viscometer at 25 °C using 96% H$_2$SO$_4$ as a solvent, and the concentration of the polymer solution was 0.01 g mL^{-1}. The intrinsic viscosity ($[\eta]$) was calculated according to eqn (1).

$$[\eta] = \frac{\sqrt{2(\eta_{sp} - \ln \eta_r)}}{C} \tag{1}$$

where C is the concentration of the solution, η_{sp} is the specific viscosity, and $\eta_{sp} = \eta_r - 1$. The viscosity-average molecular weight ($\overline{M_\eta}$) was calculated according to the Mark–Houwink equation, as shown in eqn (2).

$$[\eta] = K\overline{M_\eta}^{\alpha} \tag{2}$$

where K and α are constants that depend on the properties of the polymer solution, and their values refer to the values of PA6, which were 2.26×10^{-4} and 0.82, respectively.[27]

GPC measurement was performed on an Agilent 1260 Infinity II (USA) at 40 °C, with chromatogen-grade hexafluoroisopropanol (HFIP) as the mobile phase and a flow rate of 1.0 mL min^{-1}. Prior to the test, a narrow distribution polystyrene (PS) calibration standard curve was established.

TGA measurement was carried out on a Netzsch TG 209 F1 Libra (Germany) in a nitrogen atmosphere at a heating rate of 10 °C min^{-1} from room temperature to 800 °C.

DSC measurement was performed on a TA Q20 (USA) in a nitrogen atmosphere. The temperature was raised from 25 to 300 °C at a rate of 10 °C min^{-1}, kept at 300 °C for 5 min to eliminate thermal history, and then lowered to 25 °C at a rate of 5 °C min^{-1}, 10 °C min^{-1}, 15 °C min^{-1}, 20 °C min^{-1} and 30 °C min^{-1}, respectively. The degree of crystallinity (X_c) can be calculated according to eqn (3).

$$X_c = \frac{\Delta H_m}{\Delta H_0} \times 100\% \tag{3}$$

where ΔH_m is the melting enthalpy of the sample, and ΔH_0 is the theoretical melting enthalpy of fully crystalline PA66, which is 194.69 J g^{-1}.[28]

The tensile properties were measured according to GB/T 1040-2018 using a Sans CMT 4104 electronic universal testing machine (China) at a crosshead speed of 20 mm min^{-1}. The test was performed at room temperature, and the average value of at least five tests was calculated together with the standard deviation.

Results and discussion

Structural characterization

The chemical structures of PA66/MACM6 copolymers were characterized by FTIR. As shown in Fig. 2(a), the absorption peak at 3300 cm^{-1} corresponds to the N–H bond stretching vibration. The peak at 3080 cm^{-1} is attributed to the overtone of the N–H bending vibration. Absorption peaks at 2933 cm^{-1} and 2859 cm^{-1} represent the asymmetric and symmetric stretching vibrations of methylene groups, respectively. The peak at 1636 cm^{-1} corresponds to the C=O stretching vibration, belonging to the amide I band. At 1539 cm^{-1}, a combination absorption peak of C–H bending vibration and C–N stretching vibration appears, also known as the amide II band. The peak at 1465 cm^{-1} is assigned to the bending vibration of methylene (–CH$_2$–) groups. At 1276 cm^{-1}, a combination absorption peak of C–N stretching vibration and C–H bending vibration is observed, which belongs to the amide III band. The presence of amide I, II, and III bands confirms that all the samples possess a typical polyamide structure. In addition, with the increase in
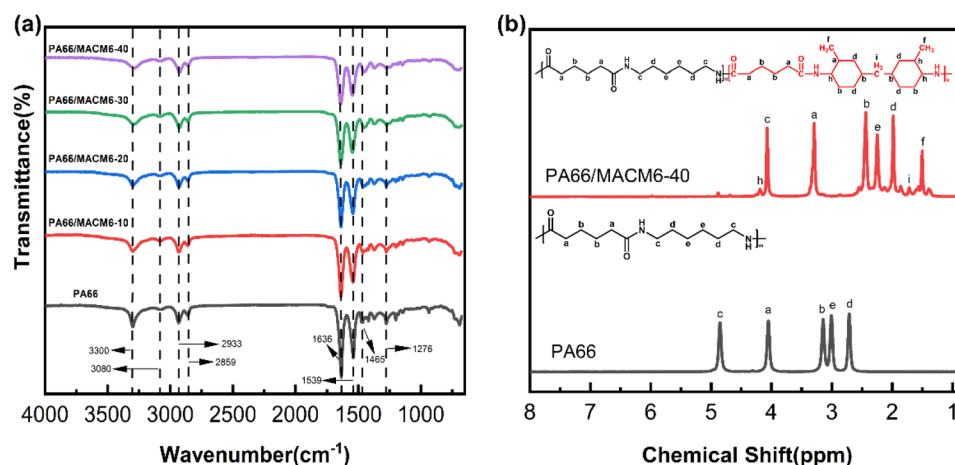

Fig. 2 FTIR spectra (a) and ^{1}H-NMR spectra (b) of PA66 and PA66/MACM6 copolymers.

the MACM6 content in the copolymer, the intensities of the N–H bond stretching vibration peak and amide I–III bands absorption peaks gradually decrease, and these peaks shift towards low wavenumbers, which indicate that the introduction of the MACM6 segment into the PA66 chain weakens the intermolecular hydrogen bond interaction of the copolymers.

To further confirm their chemical structures, ^{1}H-NMR analysis was performed. The ^{1}H-NMR spectrum of PA66/MACM6-40 in CF_3CO_2D was analyzed as a typical example, as shown in Fig. 2(b). The appearance of the characteristic proton peaks of the methyl group on the cyclohexyl ring (denoted f) and methylene group between two cyclohexyl rings (denoted i) confirms that the MACM6 segment was successfully introduced into the PA66 chain by the copolymerization method. Compared with PA66, it is found that the proton peaks of the PA66/MACM6 copolymer move to the region of low chemical shift due to the influence of the alicyclic structure, which is consistent with the FTIR result.

Molecular weight characterization data of PA66 and PA66/MACM6 copolymers obtained by viscosity method and GPC are listed in Table 1. All the samples have high molecular weight ($\overline{M_n} \geq 18831$) and narrow polydispersity index (PDI ≤ 1.75), and these data are controlled within a relatively small variation range as much as possible to reduce the impact of molecular weight differences on their properties.

Thermal properties

The thermogravimetric analysis (TGA) curves and derivative thermogravimetric (DTG) curves of PA66/MACM6 copolymers are

Table 1 Molecular weight characterization data of PA66 and PA66/MACM6 copolymers

Samples	η_r	$[\eta]$ (dL g^{-1})	$\overline{M_\eta}$	$\overline{M_n}$	$\overline{M_w}$	PDI
PA66	2.19	0.90	24 611	19 216	33 604	1.75
PA66/MACM6-10	2.20	0.91	24 810	19 660	34 138	1.74
PA66/MACM6-20	2.16	0.88	24 007	18 831	32 444	1.72
PA66/MACM6-30	2.23	0.93	25 411	21 143	35 851	1.70
PA66/MACM6-40	2.22	0.92	25 212	20 441	35 267	1.73

shown in Fig. 3, and the relevant data are summarized in Table 2. It can be observed that the TGA curves of PA66/MACM6 copolymers are essentially similar to that of PA66, with all the samples exhibiting only one weight loss step in their thermal degradation profiles. The initial thermal decomposition temperatures at 5% weight loss ($T_{5\%}$) and maximum thermal decomposition rate temperatures (T_{max}) of the PA66/MACM6 copolymers range from 374.2 °C to 388.5 °C, and 439.2 °C to 442.3 °C, respectively. These results indicate that PA66/MACM6 copolymers have good thermal stabilities, and the existence of alicyclic structure has no significant effect on their thermal stabilities.

Fig. 4 illustrates the DSC curves of PA66/MACM6 copolymers during the first cooling and the second heating process at a rate of 10 °C min^{-1}, and the corresponding data are listed in Table 2. Note that the crystallization temperature (T_c), melting point (T_m) and crystallinity (X_c) of the PA66/MACM6 copolymer are lower than those of pure PA66 and gradually decrease with the increase in the MACM6 content. This phenomenon is attributed to the steric hindrance effect of the MACM6 segment, which has large alicyclic structures with side methyl groups. The introduction of the MACM6 segment into the PA66 chain disrupts the ordered arrangement of the original molecular chain, resulting in structural irregularity and defect in the copolymer crystal. When the content of MACM6 reaches 40 wt%, the PA66/MACM6-40 copolymer exhibits the lowest T_c of 151.7 °C, the lowest T_m of 223.9 °C and the lowest crystallinity of 15.1%, indicating that the PA66/MACM6-40 copolymer has the poorest structural order. This result is also supported by the appearance of a cold crystallization peak in the second heating DSC curve of the PA66/MACM6-40 copolymer, whose molecular chain rearranges and crystallizes when the temperature rises above the glass transition temperature due to its highly disordered sequence structure.[29] Interestingly, the T_m value of pure PA66 is 264.2 °C, whereas the T_m values of the PA66/MACM6 copolymer ranges from 223.9 °C to 254.8 °C. Therefore, introducing the MACM6 segment with different contents into the PA66 chain through copolymerization is a simple and effective method to obtain rearranged sequence structures and adjustable thermal properties, and the PA66/MACM6 copolymerization system has
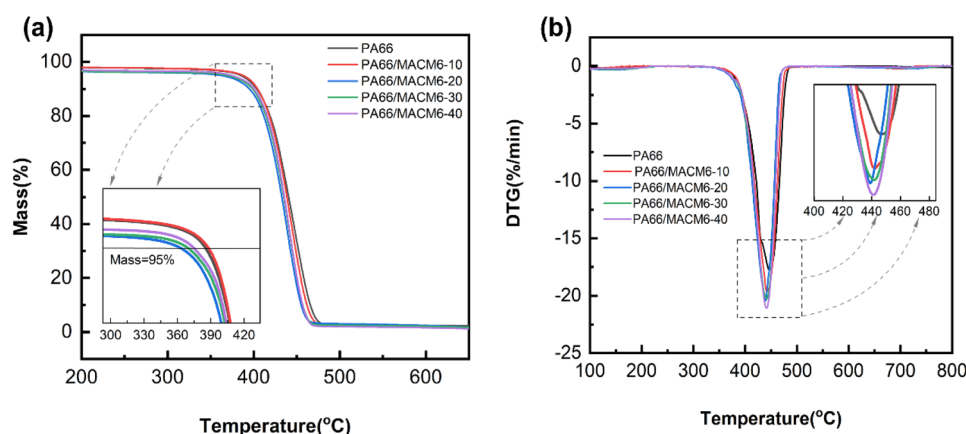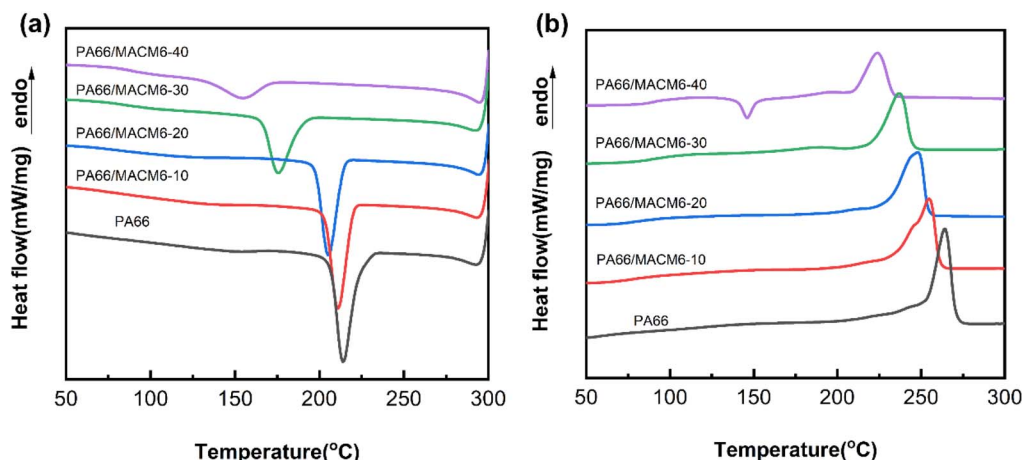

Fig. 3 TGA curves (a) and DTG curves (b) of PA66 and PA66/MACM6 copolymers.

Table 2 TGA and DSC data of PA66 and PA66/MACM6 copolymers

Samples	$T_{5\%}$ (°C)	T_{max} (°C)	T_c (°C)	T_m (°C)	ΔH_m (J g^{-1})	X_c (%)
PA66	385.6	446.7	214.0	264.2	74.1	38.1
PA66/MACM6-10	388.5	442.3	211.2	254.8	68.4	35.1
PA66/MACM6-20	374.2	439.2	205.3	248.1	60.5	31.1
PA66/MACM6-30	380.6	442.0	175.7	237.0	42.2	21.7
PA66/MACM6-40	386.3	441.2	154.3	223.9	29.4	15.1

Fig. 4 DSC curves of PA66 and PA66/MACM6 copolymers during the first cooling (a) and the second heating (b) process at a rate of 10 °C min^{-1}.

a wide tunable melting point range and can be processed in a wide temperature range to meet the requirements of different industrial applications.

Non-isothermal crystallization behaviors

Non-isothermal crystallization curves of PA66/MACM6 copolymers at different cooling rates are shown in Fig. 5. With an increase in the cooling rate, the crystallization peaks of all the samples shift towards the low temperature region and widen due to the crystallization hysteresis caused by high cooling rate. At a high cooling rate, molecular chains do not have enough time to form an ordered arrangement at high temperature; thus, the crystallization temperature decreases. Moreover, the sample at a high cooling rate has a short residence time at both
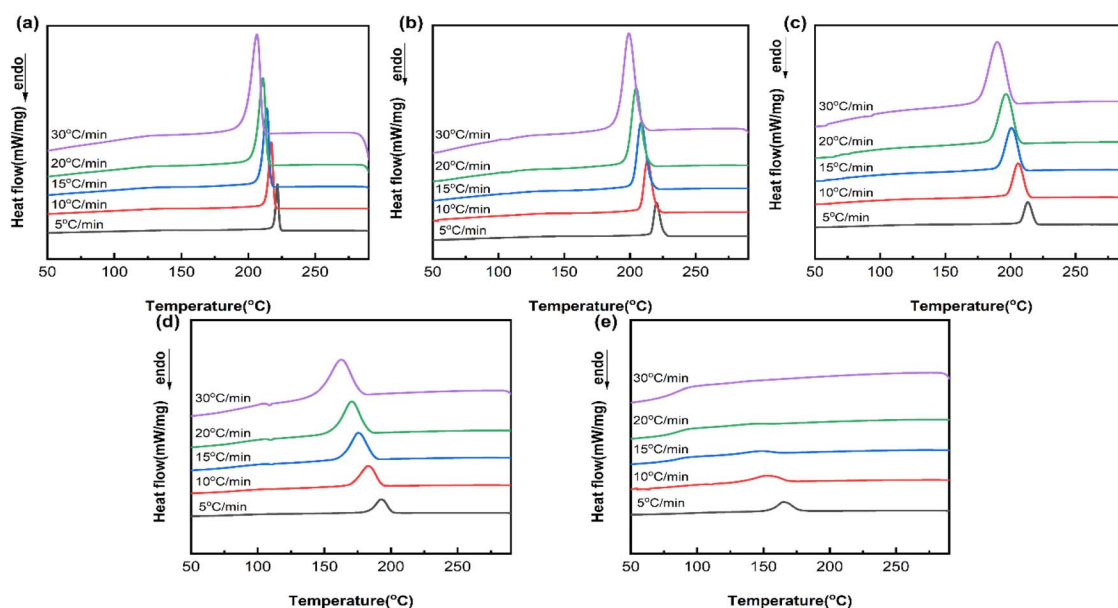

Fig. 5 Non-isothermal crystallization curves of PA66 and PA66/MACM6 copolymers at different cooling rates: (a) PA66, (b) PA66/MACM6-10, (c) PA66/MACM6-20, (d) PA66/MACM6-30, (e) PA66/MACM6-40.
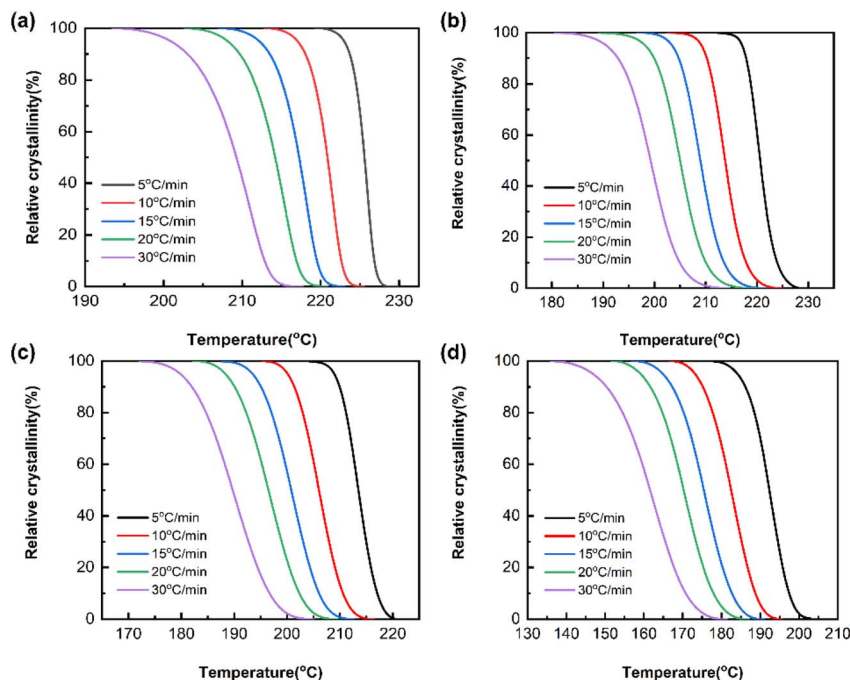
Fig. 6 $X(T){-}T$ curves of PA66 and PA66/MACM6 copolymers: (a) PA66, (b) PA66/MACM6-10, (c) PA66/MACM6-20, (d) PA66/MACM6-30.

high and low temperatures and lacks sufficient time for the formation of crystal nuclei and the growth of the crystal, resulting in high crystallization imperfection and a wide crystallization peak. At the same cooling rate, the crystallization peak of the PA66/MACM6 copolymer also moves to the low temperature region and widens with the increase in the MACM6 content. As the content of MACM6 is 40 wt%, the PA66/MACM6-40 copolymer has wide and weak crystallization peaks only at low cooling rates, and its crystallization peak disappears when the cooling rate reaches 20 °C min^{-1} or above. This is because

the PA66/MACM6-40 copolymer with high MACM6 content has low crystallization ability, and its molecular chains do not have time to regularly arrange and crystallize at high cooling rates, resulting in an amorphous structure. Therefore, the PA66/MACM6-40 copolymer was not analyzed in subsequent non-isothermal crystallization studies.

The relative crystallinity $X(T)$ of the PA66/MACM6 copolymer can be determined by the ratio of the area of the crystallization curve formed at a certain crystallization temperature to the area

Table 3 Non-isothermal crystallization kinetic parameters of PA66 and PA66/MACM6 copolymers

Samples	Φ (°C min^{-1})	T_0 (°C)	T_p (°C)	T_e (°C)	ΔT_c (°C)	$t_{1/2}$ (min)
PA66	5	218.04	221.76	224.10	6.06	0.73
	10	210.86	217.17	220.23	9.37	0.51
	15	205.27	213.76	217.51	12.24	0.40
	20	200.76	210.98	215.47	14.71	0.36
	30	193.38	206.48	211.80	18.42	0.29
PA66/MACM6-10	5	215.13	220.20	228.43	13.30	1.62
	10	206.83	213.30	222.92	16.09	1.04
	15	200.49	208.51	218.54	18.05	0.79
	20	195.43	204.60	215.33	19.90	0.66
	30	187.13	199.22	210.49	23.36	0.51
PA66/MACM6-20	5	206.84	213.12	220.12	13.28	1.84
	10	197.22	205.85	214.81	17.59	1.11
	15	190.37	200.86	210.49	20.12	0.88
	20	184.57	196.52	206.99	22.42	0.74
	30	175.23	189.80	202.54	27.31	0.52
PA66/MACM6-30	5	182.25	192.53	201.52	23.27	2.45
	10	169.22	183.02	193.74	24.52	1.31
	15	160.32	175.92	188.80	28.48	1.04
	20	153.69	170.28	184.48	30.79	0.84
	30	143.33	163.04	178.18	34.85	0.66

of the entire crystallization peak, which can be calculated according to eqn (4).

$$X(T) = \frac{A_T}{A_e} = \frac{\int_{T_0}^{T}\left(\frac{\mathrm{d}H_c}{\mathrm{d}T}\right)\mathrm{d}T}{\int_{T_0}^{T_e}\left(\frac{\mathrm{d}H_c}{\mathrm{d}T}\right)\mathrm{d}T} \qquad (4)$$

where $X(T)$ and $\mathrm{d}H_c/\mathrm{d}T$ are the relative crystallinity and heat flow at a certain crystallization temperature T, respectively; T_0 is the onset crystallization temperature, and T_e is the end crystallization temperature; A_T and A_e are the crystallization peak areas from T_0 to T and from T_0 to T_e, respectively. The $X(T)$–T curves of the PA66/MACM6 copolymers at different cooling rates are shown in Fig. 6, and the relevant parameters are listed in Table 3. The parameter Φ is the cooling rate, and ΔT_c is the temperature interval between T_0 and T_e. As the cooling rate increases, the T_0 and T_e values of each sample both decrease, and the ΔT_c value increases, which is consistent with the previous analysis of non-isothermal crystallization curves, indicating that crystallization hysteresis is caused by a high cooling rate. Moreover, at the same cooling rate, the ΔT_c values of the PA66/MACM6 copolymers are obviously higher than those of pure PA66, indicating that the addition of the MACM6 segment disrupts the regularity of PA66 molecular chains, and the steric hindrance effect caused by the large alicyclic structures with side methyl groups hinders the ordered arrangement of PA66 molecular chains. As a result, PA66/MACM6 copolymers need lower crystallization temperatures and longer crystallization times.

In the non-isothermal crystallization process, the crystallization temperature T can be converted into crystallization time t according to eqn (5).

$$t = \frac{T_0 - T}{\Phi} \qquad (5)$$

$X(t)$ is the relative crystallinity at a certain crystallization time t, and the curves of $X(t)$ with time t can be obtained by eqn (4) and (5). As shown in Fig. 7, all the $X(t)$–t curves exhibit an "S" shape and have two non-linear stages in the early and late periods of crystallization. In the early stage, nucleation is difficult due to the rapid motion of the molecular chain at high temperature, resulting in a slow crystallization rate. In the late stage, molecular chain movement is inhibited at low temperature, and the crystal growth rate decreases, leading to a decrease in the crystallization rate.[30] In addition, the higher the cooling rate, the shorter the time required to complete the crystallization. This is because the higher cooling rate leads to greater supercooling, thus allowing less time for crystallization. The half-crystallization time $t_{1/2}$ is defined as the time from the onset crystallization until the relative crystallinity $X(t)$ reaches 50%, which is an important parameter reflecting the crystallization rate of polymer materials. The $t_{1/2}$ values can be obtained from the $X(t)$–t curves, as listed in Table 3. With the increase in cooling rate, the $t_{1/2}$ value of each sample becomes shorter, indicating that the crystallization rate becomes faster at higher cooling rate. At the same cooling rate, the $t_{1/2}$ values of the PA66/MACM6 copolymers are greater than those of pure PA66 and exhibit an increasing trend with an increase in the MACM6 content. The results show that the introduction of a large
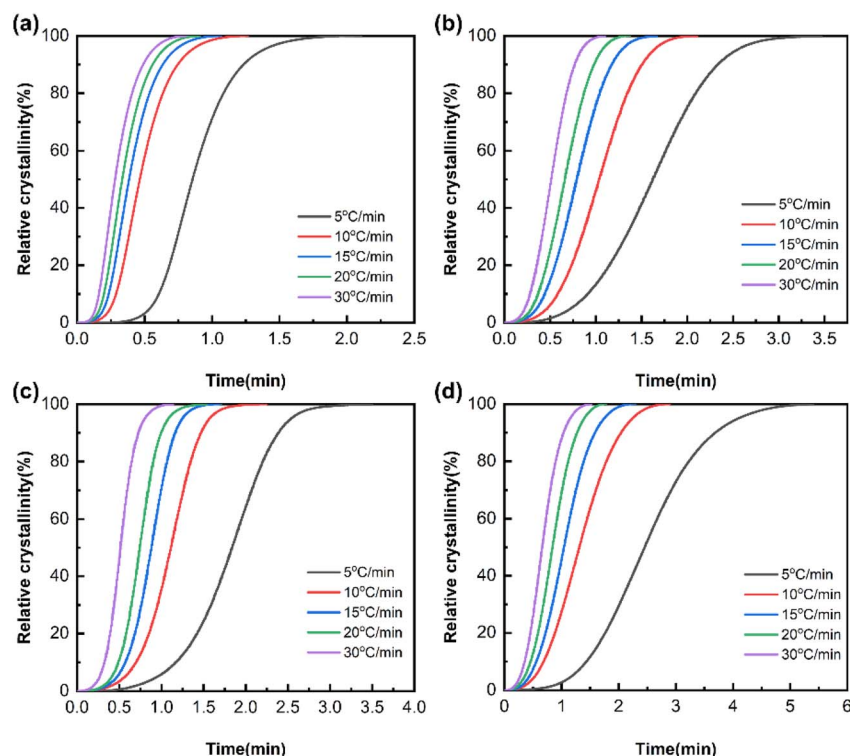

Fig. 7 $X(t)$–t curves of PA66 and PA66/MACM6 copolymers: (a) PA66, (b) PA66/MACM6-10, (c) PA66/MACM6-20, (d) PA66/MACM6-30.

MACM6 segment in the PA66 chain reduces the crystallization rate, and the higher the content of MACM6, the slower the crystallization rate. Therefore, the content of MACM6 has a great influence on the crystallization behaviors of PA66/MACM6 copolymers.

Non-isothermal crystallization kinetics

In general, the classical Avrami equation is one of the most commonly used methods for investigating the early stage of polymer isothermal crystallization kinetics, as shown in eqn (6).[31]

$$X(t) = 1 - \exp(-Z_t t^n) \qquad (6)$$

where $X(t)$ is the relative crystallinity at time t, n is the Avrami index, and Z_t is the crystallization rate constant. Taking the natural logarithm of both sides of the Avrami equation, we can obtain eqn (7).

$$\lg\{-\ln[1 - X(t)]\} = \lg Z_t + n \lg t \qquad (7)$$

In order to analyze the non-isothermal crystallization kinetics of the polymers, Jeziorny proposed[32] that the early stage of non-isothermal crystallization can be simplified by the Avrami equation at a constant cooling rate, and the non-isothermal crystallization process can be decomposed into countless isothermal crystallization processes at different temperatures. The isothermal crystallization parameter Z_t in the Avrami equation is modified to the non-isothermal crystallization parameter Z_c using eqn (8).

$$\lg Z_c = \lg Z_t / \Phi \qquad (8)$$

where Φ is the cooling rate and Z_c is the non-isothermal crystallization rate constant. The plot of $\lg\{-\ln[1 - X(t)]\}$ versus $\lg t$ is shown in Fig. 8. It can be observed that the crystallization kinetics curves for all the samples do not exhibit a perfectly linear relationship. However, they maintain good linearity within the main crystallization region. For the linear fitting of this part of data, the values of n and Z_c can be calculated through the slope and intercept, as presented in Table 4.

The Avrami index n is an important parameter reflecting the nucleation and crystal growth mechanism during polymer crystallization. When the n values range from 1 to 2, 2 to 3, 3 to 4, and more than 4, the primary modes of crystal growth are one-dimensional fibrillar, two-dimensional lamellar, three-dimensional spherulitic and complex multi-dimensional process, respectively.[30] The n values of the samples are listed in Table 4, and non-integer n values suggest that the actual crystallization process involves very complex nucleation and crystal growth mechanisms. Note that the n values of PA66/MACM6 copolymers range from 2.96 to 4.26, but most of them are in the range from 2 to 3, indicating that the crystal growth of PA66/MACM6 copolymers mainly tends towards three-dimensional spherulite mode.

The parameter Z_c is often used to evaluate the crystallization rate. Usually, the higher the Z_c value, the faster the crystallization rate. As listed in Table 4, when the cooling rate increases, the Z_c value of the PA66/MACM6 copolymer gradually increases, suggesting a higher crystallization rate with an increase in the
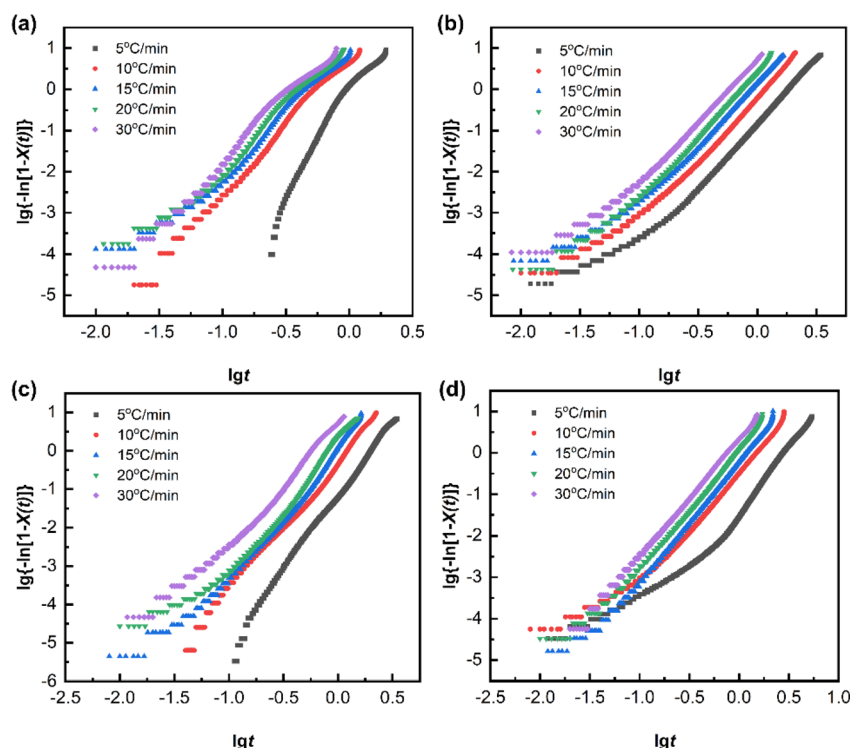

Fig. 8 $\lg\{-\ln[1 - X(t)]\}$–$\lg t$ curves of PA66 and PA66/MACM6 copolymers: (a) PA66, (b) PA66/MACM6-10, (c) PA66/MACM6-20, (d) PA66/MACM6-30.

Table 4 Non-isothermal crystallization kinetic parameters of PA66 and PA66/MACM6 copolymers based on the Jeziorny method

Samples	Φ (°C min^{-1})	n	Z_t	Z_c
PA66	5	3.69	1.175	1.033
	10	3.41	6.918	1.213
	15	3.19	10.471	1.169
	20	3.06	13.804	1.140
	30	2.78	16.982	1.099
PA66/MACM6-10	5	3.88	0.145	0.679
	10	3.76	0.617	0.953
	15	4.08	1.445	1.025
	20	4.26	2.630	1.050
	30	3.84	5.495	1.058
PA66/MACM6-20	5	3.25	0.065	0.578
	10	3.24	0.457	0.825
	15	3.20	1.135	1.009
	20	3.21	2.399	1.045
	30	3.10	8.710	1.075
PA66/MACM6-30	5	3.50	0.029	0.492
	10	2.90	0.316	0.891
	15	3.05	0.603	0.967
	20	3.01	1.140	1.007
	30	2.96	2.344	1.029

cooling rate. This variation trend is more significant at lower cooling rates (such as 5 °C min^{-1} to 15 °C min^{-1}), and small changes at higher cooling rates may be attributed to the inability of molecular chains to stack and rearrange quickly enough to respond to temperature changes at higher cooling rates. At the same cooling rate, the Z_c order of these four samples is PA66 > PA66/MACM6-10 > PA66/MACM6-20 > PA66/

MACM6-30, indicating that the crystallization rate of the sample decreases with the increase in the MACM6 content. This is consistent with the analysis results of $t_{1/2}$ mentioned above.

In order to describe the non-isothermal crystallization kinetics more accurately, Mo *et al.* proposed a new method by combining the Avrami equation with the Ozawa equation,[33] as shown in eqn (9).

$$\lg \Phi = \lg F(T) - \alpha \lg t \tag{9}$$

Here, Φ represents the cooling rate; $F(T)$ represents the cooling rate required to achieve a specific degree of crystallinity; $\alpha = n/m$, where n is the Avrami exponent and m is the Ozawa exponent. At different $X(t)$ values, scatter plots of $\lg \Phi$ *versus* $\lg t$ were created and fitted. The $\lg \Phi$–$\lg t$ curves for PA66 and PA66/MACM6 copolymers are shown in Fig. 9. The slope of these fitting lines is $-\alpha$, and the intercept is $\lg F(T)$. The fitting results are presented in Table 5. Generally, a higher $F(T)$ value means a lower crystallization rate. For the same sample, the $F(T)$ value increases with increasing $X(t)$, indicating that a higher cooling rate is required to achieve a higher degree of crystallinity in a given time.[34] At the same $X(t)$, with the increase in the MACM6 content, the $F(T)$ value of the PA66/MACM6 copolymer increases. This result further confirms that the presence of MACM6 segments reduces the crystallization rate, which is consistent with the previous conclusions. The α values for all the samples do not vary significantly within the selected range of relative crystallinity. Therefore, the Mo method successfully describes the non-isothermal crystallization behavior of the copolymers.
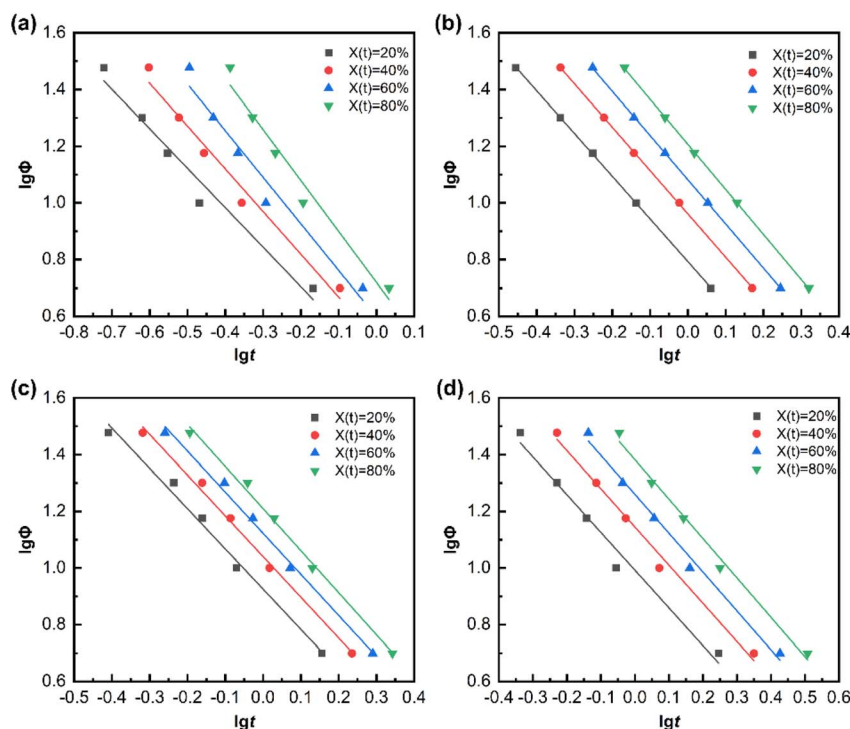

Fig. 9 $\lg \Phi$–$\lg t$ curves of PA66 and PA66/MACM6 copolymers: (a) PA66, (b) PA66/MACM6-10, (c) PA66/MACM6-20, (d) PA66/MACM6-30.

Table 5 Non-isothermal crystallization kinetic parameters of PA66 and PA66/MACM6 copolymers based on the MO method

Samples	$X(t)$ (%)	α	$F(T)$
PA66	20	1.39	2.69
	40	1.51	3.31
	60	1.64	3.98
	80	1.80	5.25
PA66/MACM6-10	20	1.51	6.17
	40	1.53	9.12
	60	1.56	12.02
	80	1.59	16.22
PA66/MACM6-20	20	1.42	8.51
	40	1.44	10.97
	60	1.45	13.18
	80	1.49	16.22
PA66/MACM6-30	20	1.33	9.77
	40	1.35	13.80
	60	1.37	18.20
	80	1.39	23.99

Non-isothermal crystallization activation energy

The crystallization process of crystalline polymers is typically controlled by two factors: the free energy barrier for crystal nucleation and the activation energy for crystal units to cross the phase interface.[35,36] The crystallization activation energy, related to the energy and barriers in the phase transition process, is a crucial parameter in phase transition. It represents the energy required to overcome the barrier during polymer crystallization, effectively reflecting the crystallization ability of the polymer.[37,38] In general, the higher the crystallization activation energy, the higher the crystallization energy barrier, and thus the lower the crystallization rate. The crystallization activation energy for non-isothermal crystallization processes can be calculated using the Kissinger equation, as shown in eqn (10).

$$\frac{d\left[\ln\left(\Phi/T_p^2\right)\right]}{d\left(1/T_p\right)} = -\frac{\Delta E}{R} \tag{10}$$

where R is the ideal gas constant, and ΔE is the crystallization activation energy. Using the data in Table 3, the fitting $\ln(\Phi/T_p^2)$–$1/T_p$ curves were obtained and are shown in Fig. 10(a), and good linear fitting results can be observed for all the samples. The ΔE values can be calculated from the slopes of these fitting curves, as shown in Fig. 10(b). Obviously, the ΔE value of each PA66/MACM6 copolymer is higher than that of pure PA66, and the ΔE value increases when the content of MACM6 increases. After the introduction of alicyclic structure into the PA66 chain by copolymerization, the molecular chain mobility and rearrangement ability decreases, the crystallization energy barrier increased, and the crystallization ability decreases.[39] Therefore, the PA66/MACM6 copolymer with high MACM6 content has high crystallization activation energy and low crystallization rate.

Mechanical properties

The tensile strength and elongation at break of PA66 and PA66/MACM6 copolymers are shown in Fig. 11(a). Compared with PA66, the tensile strength of the PA66/MACM6 copolymer
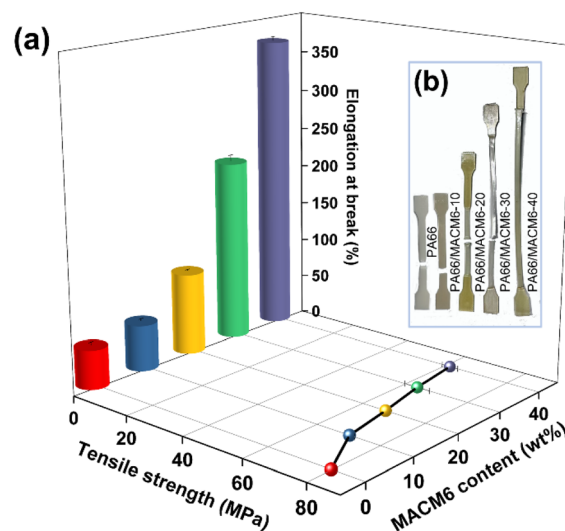
Fig. 11 Tensile properties of PA66 and PA66/MACM6 copolymers: (a) tensile strength and elongation at break, (b) specimen appearance after tensile test.
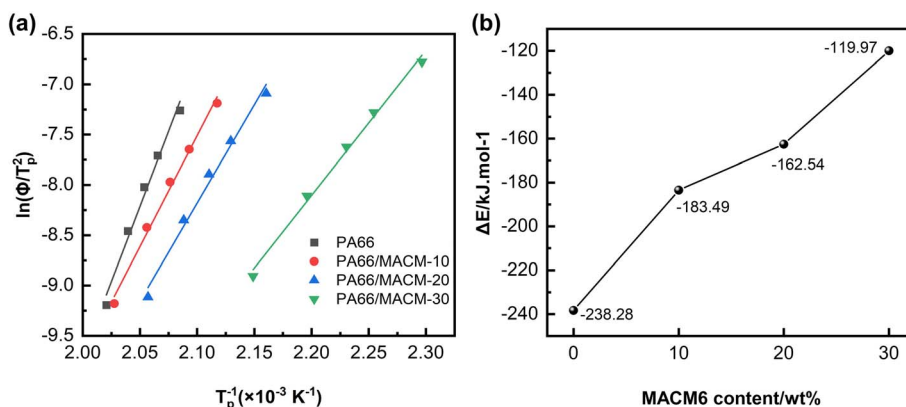
Fig. 10 $\ln(\Phi/T_p^2)$–$1/T_p$ curves (a) and crystallization activation energy data (b) of PA66 and PA66/MACM6 copolymers.

decreases slightly, but its elongation at break increases significantly. When the content of MACM6 reaches 40 wt%, the elongation at break of PA66/MACM6-40 is about 760% higher than that of PA66. The significant increase in the elongation at break indicates that PA66/MACM6 copolymers have high toughness, which is attributed to the decrease in the crystallinity due to the destruction of chain segment regularity by copolymerization. In addition, as shown in Fig. 11(b), when the content of MACM6 exceeds 20%, PA66/MACM6 copolymers exhibit obvious stress whitening and necking phenomena after tensile test, which further confirms that high toughness can be achieved by introducing alicyclic structure into PA66 chain by copolymerization.

Conclusions

In this study, PA66/MACM6 copolymers with alicyclic structures were successfully synthesized by the copolymerization of PA66 salt and MACM6 salt. TGA and DSC results indicate that PA66/MACM6 copolymers have excellent thermal stabilities with a $T_{5\%}$ above 374 °C, and their melting points range from 223.9 °C to 254.8 °C, demonstrating that copolymerization modification can improve the processing performance of PA66 without reducing its thermal stabilities. Note that the melting point, crystallization temperature and crystallinity of the PA66/MACM6 copolymer decrease gradually with the increase in MACM6 content. Moreover, the non-isothermal crystallization kinetics of PA66/MACM6 copolymers was investigated using the Jeziorny and Mo methods, suggesting that the introduction of MACM6 segments inhibited PA66 crystallization and slowed its crystallization rate. The non-isothermal crystallization activation energy was calculated using the Kissinger method. With the increase in MACM6 content, the ΔE value of the PA66/MACM6 copolymer increases gradually, making crystallization more difficult. In addition, PA66/MACM6 copolymers exhibit greatly improved toughness with a slight decrease in the strength. When the content of MACM6 reaches 40 wt%, the elongation at break of PA66/MACM6-40 is about 760% higher than that of PA66, showing high toughness. In summary, the content of MACM6 has great influence on the structures and properties of PA66/MACM6 copolymers. Therefore, it is a simple and effective method to adjust the thermal properties, crystallization behaviors and mechanical properties of the PA66/MACM6 copolymer by changing the content of MACM6 to meet the requirements of different industrial applications. This work provides a promising pathway for the synthesis of polyamide materials with desired properties.

Data availability

The data supporting this work can be obtained from the corresponding author upon request.

Author contributions

Methodology, W. L., C. W., Y. Y., J. L. and M. L.; validation, C. W.; investigation, W. L., Y. Y., J. L., M. L. and W. W.; resources, W. W.; data curation, W. L.; writing—original draft, W. L.; writing—review & editing, C. W.; supervision, W. W.

Conflicts of interest

The authors have declared there exist no competing interests.

References

1 Z. Zhan, J. Shi, Y. Zhang, Y. Zhang, B. Zhang and W. Liu, The study on flame retardancy synergetic mechanism of magnesium oxide for PA66/AlPi composite, *Mater. Res. Express*, 2019, **6**, 115317.

2 Y. L. Li, X. M. Hao, Y. F. Guo, X. Chen, Y. Yang and J. M. Wang, Study on the Acid Resistant Properties of Bio-Based Nylon 56 Fiber Compared with the Fiber of Nylon 6 and Nylon 66, *Adv. Mater. Res.*, 2014, **1048**, 57–61.

3 Z. Zhan, M. Xu and B. Li, Synergistic effects of sepiolite on the flame retardant properties and thermal degradation behaviors of polyamide 66/aluminum diethylphosphinate composites, *Polym. Degrad. Stab.*, 2015, **117**, 66–74.

4 X. Yang, Q. Li, Z. Chen, H. Han and H. Jing, Mechanical Properties and Flame Retardancy Research of Montmorillonite Intercalate Polyamide 66 Composites, *J. Compos. Mater.*, 2009, **43**, 2785–2792.

5 W. Lyu, Y. Cui, X. Zhang, J. Yuan and W. Zhang, Synthesis, thermal stability, and flame retardancy of PA66, treated with dichlorophenylphsophine derivatives, *Des. Monomers Polym.*, 2016, **19**, 420–428.

6 E. Chi, Y. Tang and Z. Wang, In Situ SAXS and WAXD Investigations of Polyamide 66/Reduced Graphene Oxide Nanocomposites During Uniaxial Deformation, *ACS Omega*, 2021, **6**, 11762–11771.

7 J. Ning, C. Tian, Y. Yang, L. Huang, J. Lv, F. Zeng, Q. Liu, F. Zhao, W. Kong and X. Cai, A novel intrinsic semi-aromatic polyamide dielectric toward excellent thermal stability, mechanical robustness and dielectric performance, *Polymer*, 2021, **234**, 124233.

8 Y. Liu, M. Xu, R. Zhang, D. Hu, L. Zhang and L. Zhao, Simultaneous Enhancement of the Conductivity and Toughness for Polyamide 66 Nanocomposites by Regulating the Hydrogen Bond and Introducing Microcellular Structures, *ACS Appl. Polym. Mater.*, 2024, **6**, 10526–10534.

9 J. Lu, Q. Ma, J. Yao, J. Yin, R. Zhang and F. Luo, Toughness enhancement of polyamide 1012 with intermolecular hydrogen bonding with 3-pentadecylphenol, *eXPRESS Polym. Lett.*, 2024, **18**, 705–714.

10 M. Odrobina, T. Deák, L. Székely, T. Mankovits, R. Z. Keresztes and G. Kalácska, The Effect of Crystallinity on the Toughness of Cast Polyamide 6 Rods with Different Diameters, *Polymers*, 2020, **12**, 293.

11 H. Sun, Z. Fang, T. Li, F. Lei, F. Jiang, D. Li, Y. Zhou and D. Sun, Enhanced mechanical and tribological performance of PA66 nanocomposites containing 2D layered α-zirconium phosphate nanoplatelets with different sizes, *Adv. Compos. Hybrid Mater.*, 2019, **2**, 407–422.

12 J. Tang, B. Xu, Z. Xi, X. Pan and L. Zhao, Controllable Crystallization Behavior of Nylon-6/66 Copolymers Based on Regulating Sequence Distribution, *Ind. Eng. Chem. Res.*, 2018, **57**, 15008–15019.

13 E. D. Harvey and F. J. Hybart, Rates of crystallization of copolyamides. II. Random copolymers of nylons 66 and 6, *J. Appl. Polym. Sci.*, 1970, **14**, 2133–2143.

14 N. Lin, Z. Wang, H. Kang, X. Hao and R. Liu, Synthesis and characterizations of random copolyamide PA(56-co-66): excellent toughness and transparency, *Polymer*, 2024, **307**, 127271.

15 S.-P. Rwei, Y.-C. Tseng, K.-C. Chiu, S.-M. Chang and Y.-M. Chen, The crystallization kinetics of nylon 6/6T and nylon 66/6T copolymers, *Thermochim. Acta*, 2013, **555**, 37–45.

16 Y.-H. Chen, P. Ranganathan, Y.-H. Lee and S.-P. Rwei, New Strategy and Polymer Design to Synthesize Polyamide 66 (PA66) Copolymers with Aromatic Moieties from Recycled PET (rPET), *ACS Sustainable Chem. Eng.*, 2021, **9**, 3518–3528.

17 J. Li, Y. Yi, C. Wang, W. Lu, M. Liao, X. Jing and W. Wang, An Intrinsically Transparent Polyamide Film with Superior Toughness and Great Optical Performance, *Polymers*, 2024, **16**, 599.

18 C.-H. Tseng and P.-S. Tsai, The Isothermal and Nonisothermal Crystallization Kinetics and Morphology of Solvent-Precipitated Nylon 66, *Polymers*, 2022, **14**, 442.

19 X. Sun, K. Mai, C. Zhang, M. Cao, Y. Zhang and X. Zhang, Nonisothermal crystallization kinetics of bio-based semi-aromatic polyamides, *J. Therm. Anal. Calorim.*, 2017, **130**, 1021–1030.

20 R. Somsunan and N. Mainoiy, Isothermal and non-isothermal crystallization kinetics of PLA/PBS blends with talc as nucleating agent, *J. Therm. Anal. Calorim.*, 2020, **139**, 1941–1948.

21 J. Shi, X. Yang, X. Wang and L. Lu, Non-isothermal crystallization kinetics of nylon 6/attapulgite nanocomposites, *Polym. Test.*, 2010, **29**, 596–602.

22 X. Fu, X. Dong, G. Yang and S. Bai, Non-isothermal crystallization kinetics of graphene/PA10T composites, *Heliyon*, 2022, **8**, e10206.

23 Y. Wang, H. Kang, R. Wang, R. Liu and X. Hao, Crystallization of polyamide 56/polyamide 66 blends: non-isothermal crystallization kinetics, *J. Appl. Polym. Sci.*, 2018, **135**, 46409.

24 D. Gan, Y. Liu, T. Hu, S. Fan, X. Liu, L. Cui, L. Yang, Y. Wu, L. Chen and Z. Mo, The Investigation of Copolymer Composition Sequence on Non-Isothermal Crystallization Kinetics of Bio-Based Polyamide 56/512, *Polymers*, 2023, **15**, 2345.

25 A. Layachi, D. Frihi, H. Satha, R. Seguela and S. Gherib, Non-isothermal crystallization kinetics of polyamide 66/glass fibers/carbon black composites, *J. Therm. Anal. Calorim.*, 2016, **124**, 1319–1329.

26 B. Liu, G. Hu, J. Zhang and Z. Wang, The non-isothermal crystallization behavior of polyamide 6 and polyamide 6/ HDPE/MAH/L-101 composites, *J. Polym. Eng.*, 2019, **39**, 124–133.

27 K. Shi, L. Ye and G. Li, Thermal oxidative aging behavior and stabilizing mechanism of highly oriented polyamide 6, *J. Therm. Anal. Calorim.*, 2016, **126**, 795–805.

28 Y. Zhang, Y. Liu and Q. Wang, Synergistic effect of melamine polyphosphate with macromolecular charring agent novolac in wollastonite filled PA66, *J. Appl. Polym. Sci.*, 2010, **116**, 45–49.

29 Y. Haoyu, Z. Xiaoqi, L. Yiming, M. Lu, H. Suqin, H. Miaoming, L. Hao, X. Wanlin and L. Wentao, Synthesis and comprehensive characterization of bio-based polyamide 56/6 copolymer: mechanical, thermal, and processing properties, *Eur. Polym. J.*, 2024, **202**, 112593.

30 J. Lagarinhos, S. Magalhães Da Silva and J. M. Oliveira, Non-Isothermal Crystallization Kinetics of Polyamide 6/Graphene Nanoplatelets Nanocomposites Obtained via In Situ Polymerization: Effect of Nanofiller Size, *Polymers*, 2023, **15**, 4109.

31 M. Avrami, Kinetics of Phase Change. I General Theory, *J. Chem. Phys.*, 1939, **7**, 1103–1112.

32 A. Jeziorny, Parameters characterizing the kinetics of the non-isothermal crystallization of poly(ethylene terephthalate) determined by d.s.c., *Polymer*, 1978, **19**, 1142–1144.

33 T. Liu, Z. Mo and H. Zhang, Nonisothermal melt and cold crystallization kinetics of poly(aryl ether ether ketone ketone), *Polym. Eng. Sci.*, 1997, **37**, 568–575.

34 C. Meng and X. Liu, One-step method for synthesis of bio-based semi-aromatic high-temperature polyamide PA5T/56 and its non-isothermal crystallization kinetics, *J. Therm. Anal. Calorim.*, 2022, **147**, 12245–12252.

35 L. R. Melo De Lima, T. Trindade and J. M. Oliveira, Non-isothermal crystallization kinetics of poly(propylene)-based graphene nanocomposites for injection moulding, *J. Therm. Anal. Calorim.*, 2022, **147**, 14229–14240.

36 L. Fang, S. Fang, S. Zhang, Z. Su, J. Zhang and Y. Lan, Non-Isothermal Crystallization Kinetics of Polyvinylidene Fluoride (PVDF)/Microcrystalline Graphite (MCG) Composites, *J. Macromol. Sci., Part B:Phys.*, 2022, **61**, 1008–1023.

37 B. Liu, G. Hu, J. Zhang and W. Yan, Non-isothermal crystallization, yellowing resistance and mechanical properties of heat-resistant nylon 10T/66/titania dioxide/ glass fibre composites, *RSC Adv.*, 2019, **9**, 7057–7064.

38 Z. Ma, X. He, X. Cao, X. Yang, X. Jiao, Z. Hou, R. Pan and J. Cai, Analysis of the Non-isothermal Crystallization Kinetics of the Polyamide 6/M-lignin Composites, *J. Macromol. Sci., Part B:Phys.*, 2024, **63**, 930–940.

39 R. Jin, Z. Chen, Y. Ouyang, X. Lin, X. Dai, S. Zhang, R. Xu, Z. Wang and Y. Peng, Enhancing the Non-Isothermal Crystallization Kinetics of Polylactic Acid by Incorporating a Novel Nucleating Agent, *Polymers*, 2024, **16**, 3204.